JCB Journal of Cell Biology

REPORT

Nuclear transport adapts to varying heat stress in a multistep mechanism

Yutaka Ogawa and Naoko Imamoto

Appropriate cell growth conditions are limited to a narrow temperature range. Once the temperature is out of this range, cells respond to protect themselves, but temperature thresholds at which various intracellular responses occur, including nuclear transport systems, remain unclear. Using a newly developed precise temperature shift assay, we found that individual transport pathways have different sensitivities to a rise in temperature. Nuclear translocations of molecular chaperone HSP70s occur at a much lower temperature than the inhibition of Ran-dependent transport. Subsequently, importin (Imp) α/β–dependent import ceases at a lower temperature than other Ran-dependent transport, suggesting that these are controlled by independent mechanisms. In vitro research revealed that the inhibition of Imp α/β–dependent import is caused by the dysfunction of Imp α1 specifically at lower temperature. Thus, the thermosensitivity of Imp α1 modulates transport balances and enables the multistep shutdown of Ran-dependent transport systems according to the degree of heat stress.

Introduction

In eukaryotic cells, nucleocytoplasmic transport of molecules plays an important role in maintaining cellular homeostasis. All transport occurs through the nuclear pore complexes (NPCs), which are embedded in the nuclear envelope (Cronshaw et al., 2002). Translocations of macromolecules is mainly mediated by importins (Imps) and exportins (Görlich and Kutay, 1999; Weis, 2003; Stewart, 2007; Chook and Süel, 2011; Kimura and Imamoto, 2014) under the control of the GTP-bound form of Ran (RanGTP), which is abundant in the nucleus (Kalab et al., 2002; Kaláb et al., 2006).

Similar with other intracellular reactions, nuclear transport systems are affected by a variety of cellular stresses including heat, oxidative, and osmotic stresses (Furuta et al., 2004; Miyamoto et al., 2004; Kelley and Paschal, 2007; Kodiha et al., 2008; Yoshimura et al., 2013; Datta et al., 2014). In particular, high temperatures induce a variety of phases of cellular responses to cytotoxicity (Richter et al., 2010). Whereas Imp α/β–dependent import is down-regulated under high-temperature conditions, HSP70s, a major molecular chaperone (Hartl et al., 2011), translocates into the nucleus through the function of the specific import factor, Hikeshi, in a Ran-independent manner (Kose et al., 2012). However, what causes the heat-induced nuclear transport switching and the relationship among transport pathways remain unclear.

In this study, using newly developed precisely controlled temperature-shift assay methods, we analyzed relationships between nuclear transport efficiencies and temperatures and showed that nuclear translocation of HSP70s, Imp α/β–dependent import, and other Ran-dependent transport are controlled by independent mechanisms under high temperature.

Results and discussion

Most studies on heat stress responses used comparison experiments in two environments: physiological (37°C) and heat stress (42–45°C) conditions. However, the body temperature rises by only 1–2°C during febrile diseases in homeothermic animals, and different responses occur (Park et al., 2005). Therefore, to understand the mechanism of heat stress responses in detail, it is very important to conduct analysis at a series of temperatures.

For this purpose, we used a new experimental method, namely temperature shift assay, with a conventional thermal cycler (Fig. 1 a). HeLa S3 suspension cultures were added to PCR tubes, and the individual lines were subjected to a stepwise temperature gradient allowing for incubation of cells at various temperatures simultaneously. The thermal program of each line was in a stepwise temperature gradient from ∼37°C to 45°C for 60 min after 1 min of incubation at 36.8°C. As shown in Fig. 1 b, the actual temperatures of individual lines were controlled with high precision (the error at a gradient temperature step was less than ±0.1°C) and high reproducibility of temperature-increase levels. Notably, because >70% of cells incubated at 37°C survived even after 26 h (Fig. 1 c), the incubation for a few hours in the PCR tubes does not have a serious impact on cell health.

Cellular Dynamics Laboratory, RIKEN Cluster for Pioneering Research, Saitama, Japan.

Correspondence to Naoko Imamoto: nimamoto@riken.jp; Yutaka Ogawa: yogawa@riken.jp.

https://doi.org/10.1083/jcb.201712042

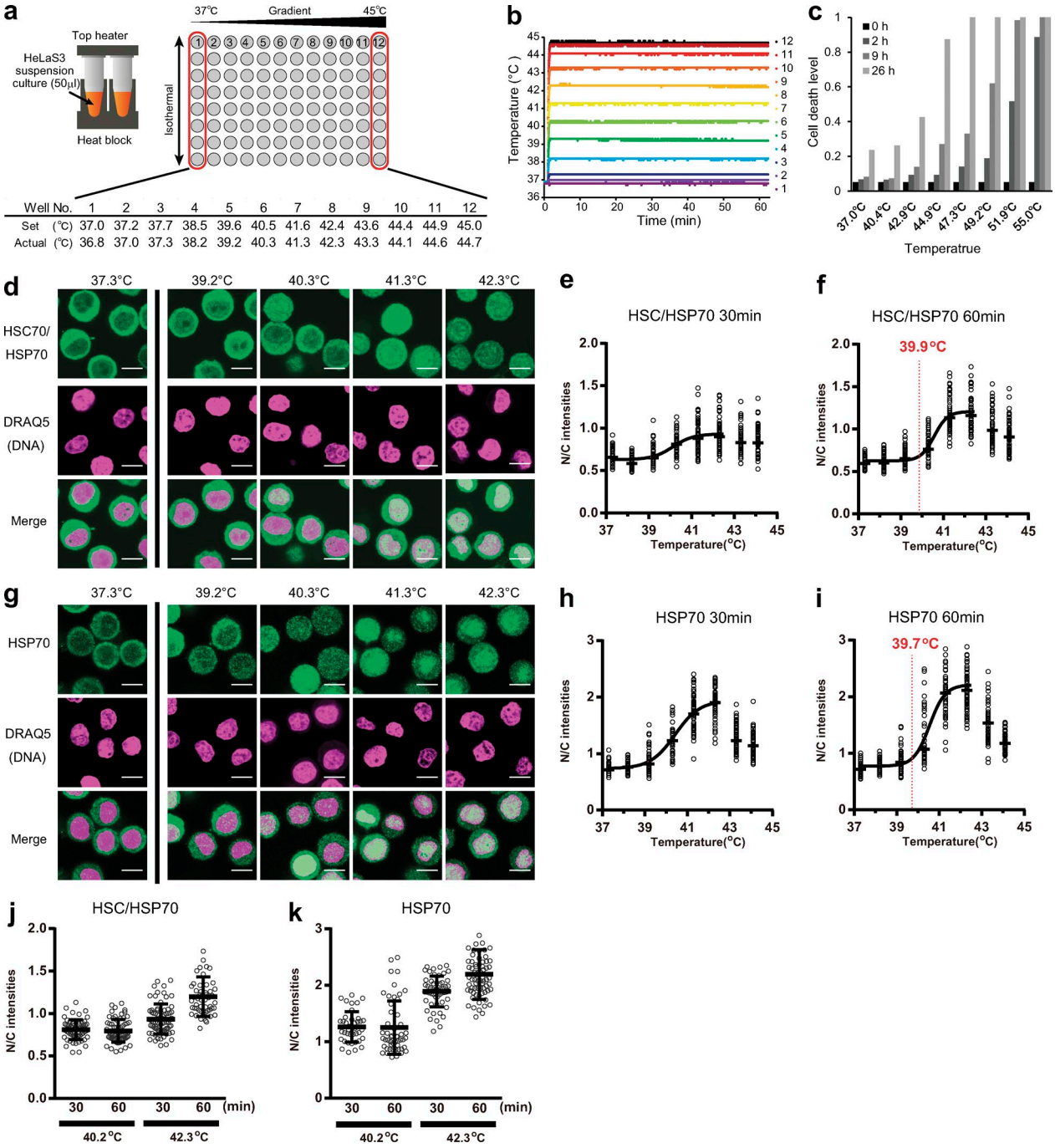

Figure 1. **Nuclear translocation of HSC/HSP70 under precise temperature control. (a)** Illustration of the temperature-shift assay system. HeLa S3 suspension culture was added in the PCR tube and placed in the thermal cycler. Set and actual temperatures of each well are shown in the table. **(b)** The temperature stability of the assay system was checked. After incubation at 36.8°C for 1 min, well temperatures were increased (36.8 to 44.7°C from left to right) and maintained. The well temperature was plotted every second over 60 min. **(c)** Cell death levels of HeLa S3 suspension culture cells in PCR tubes were checked by trypan blue exclusion tests at indicated time points (n = 877 [37.0°C], 832 [40.4°C], 822 [42.9°C], 695 [44.9°C], 471 [47.3°C], 571 [49.2°C], 515 [51.9°C], and 265 [55.0°C] in one simultaneous experiment). **(d–j)** After incubation at 36.8°C for 1 min, the cells were shifted to various temperatures and incubated for either 30 (e and h) or 60 min (d, f, g, and i). The cells were then fixed and stained with DRAQ5 and an antibody recognizing both HSC70 and HSP70 (d–f) or only HSP70 (g–i). **(d and g)** Bars, 10 µm. **(e, f, h, and i)** The mean nuclear intensities relative to mean cytoplasmic intensities (N/C intensities) are plotted. The black bars show the median of >50 cells at eight temperature conditions (total n = 514 [e], 495 [f], 502 [h], and 467 [i]). All plots in each graph were calculated from one simultaneous experiment. These plots were fitted to a sigmoid curve, and threshold temperatures were determined (red lines; see Materials and methods). **(j and k)** All plots of the N/C intensities after 30- or 60-min incubations at 39.2 or 43.3°C are shown. Error bars indicate means ± SD.

HSC70 and HSP70, constitutive and inducible members of the 70-kD heat shock protein family, are representatives of nuclear translocating proteins in response to temperature shifts (Welch and Feramisco, 1984). We first examined localization changes of endogenous HSC/HSP70 in a temperature-dependent manner. After either a 30- or 60-min period of temperature shift assay,

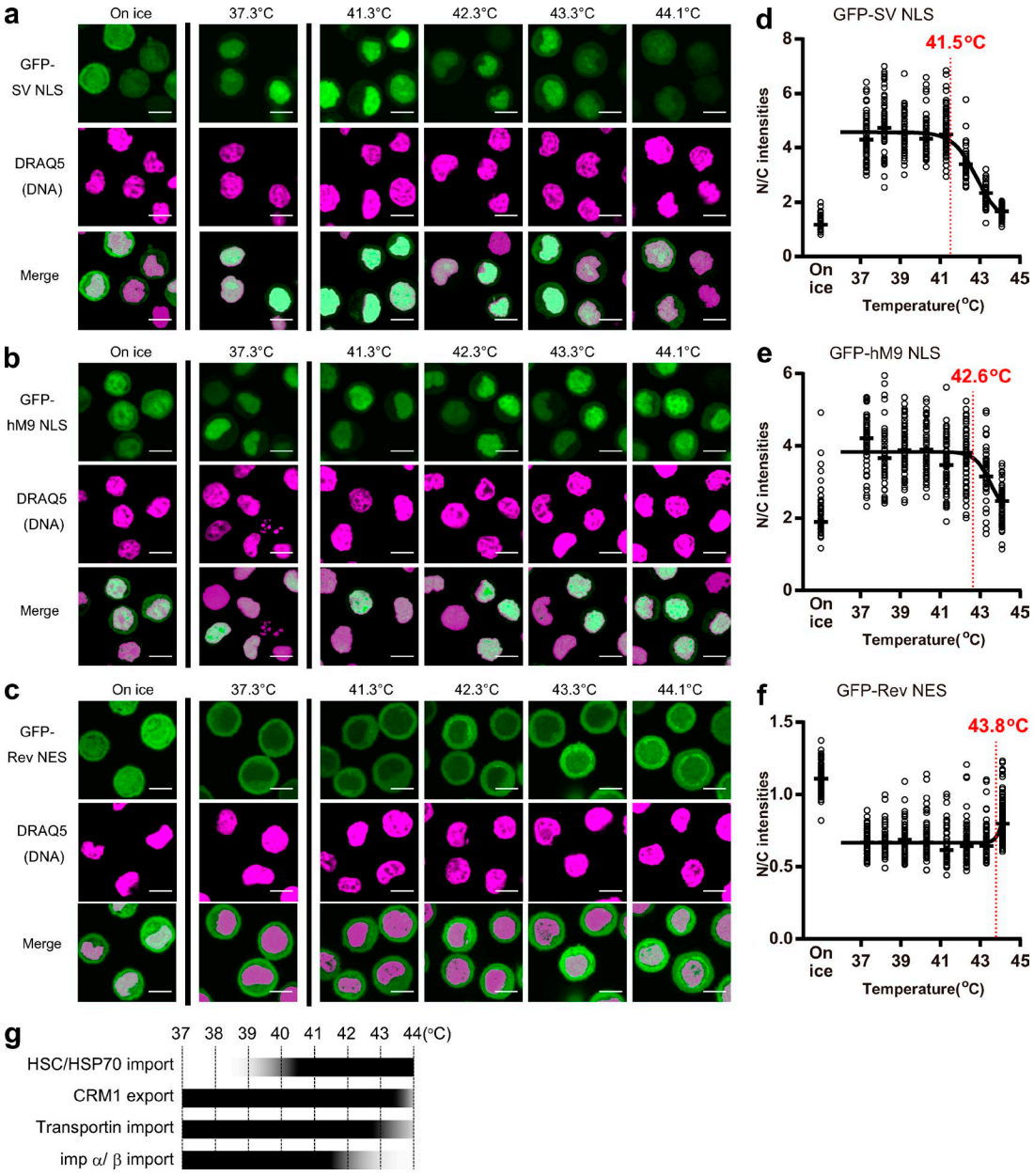

Figure 2. **Nuclear transport efficiencies in high-temperature conditions. (a–c)** After 60 min incubation at indicated temperatures, the GFP-SV NLS–(a), GFP-hM9 NLS– (b), or GFP-Rev NES (c)–expressing stable HeLa S3 cells were fixed, stained with DRAQ5, and observed. Bars, 10 µm. **(d–f)** N/C intensities of GFP-SV NLS (d), GFP-hM9 NLS (e), or GFP-Rev NES (f) at each temperature were plotted. The black bars show the median of >50 cells at nine temperature conditions (total *n* = 632 [d], 575 [e], and 952 [f]). All plots in each graph were calculated from one simultaneous experiment. Red lines show the threshold temperatures. **(g)** Overview of thermosensitivities of nuclear transport systems.

the cells were stained with an antibody that reacts with both HSC70 and HSP70. As shown in Fig. 1 d, HSC/HSP70 translocate into the nucleus depending on the temperature rise. For detailed analysis, we plotted the mean nuclear intensity versus the mean cytoplasmic intensity of HSC/HSP70 in individual cells at various temperatures (Fig. 1, e and f). HSC/HSP70 translocate into the nucleus according to the temperature rise. This was also confirmed by using the antibody reacting against only HSP70, which showed 86% sequence homology with HSC70 (Fig. 1, g–i; Daugaard et al., 2007).

Additionally, we fitted the plots to a sigmoid curve and determined threshold temperatures. The threshold temperatures from experiments using HSC/HSP70 and HSP70 antibodies matched well (39.9 and 39.7°C, respectively; Fig. 1, f and i). Notably, the localization changes of HSP70s at 40.3°C completed within 30 min. However, HSP70s continued to accumulate into the nucleus even after 30 min at 42.3°C (Fig. 1, j and k). This result implies that the amount of nuclear translocation is controlled in accordance with the degree of heat stress.

Contrary to HSP70s, Ran-dependent nuclear transport is expected to be down-regulated under high-temperature conditions. To analyze this, we established three cell lines that stably expressed GFP-fused nuclear localization signal (NLS) and nuclear export signal (NES) peptides (i.e., GFP–SV40T antigen

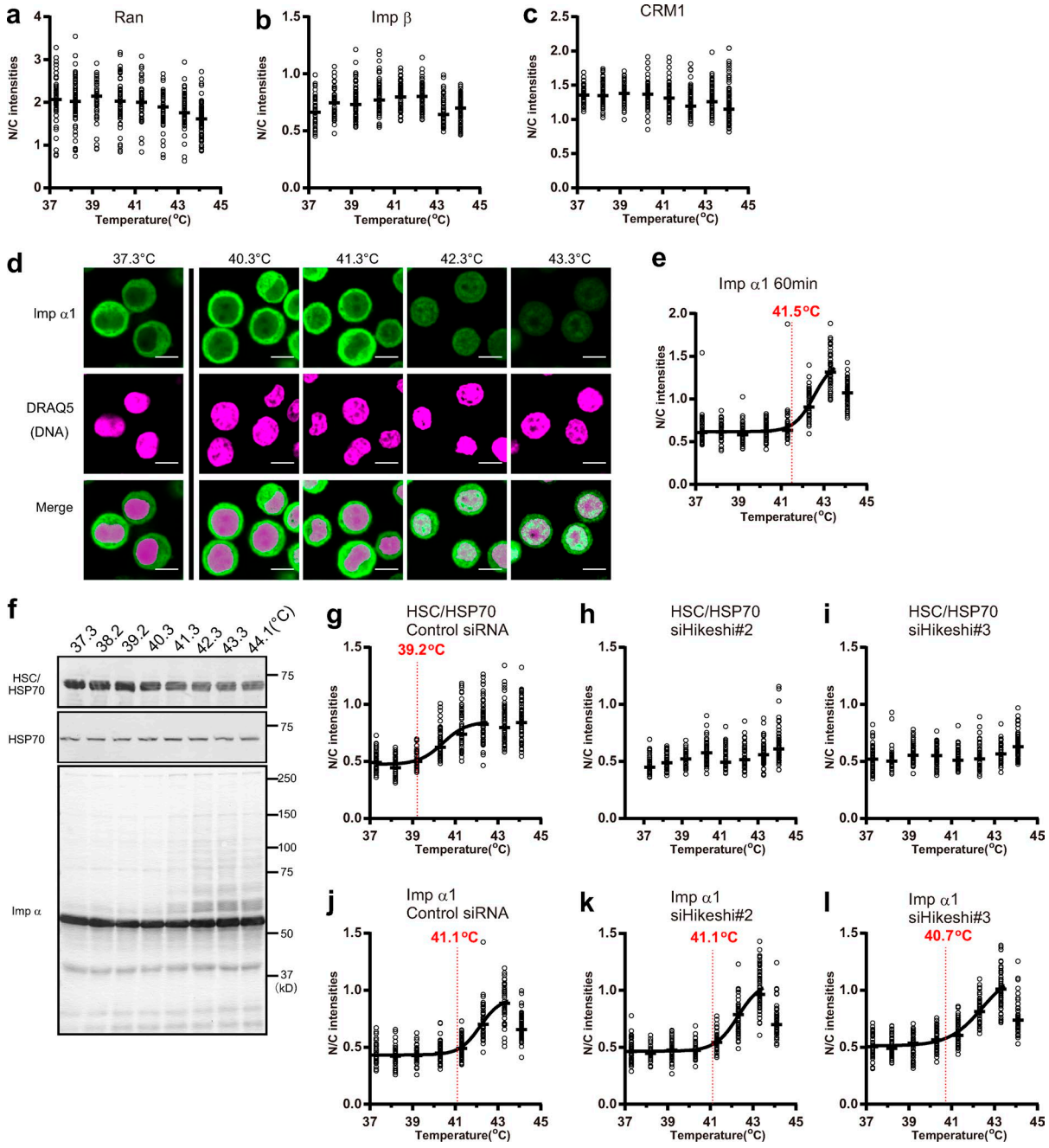

Figure 3. **Nuclear transport factors in high-temperature conditions. (a–e)** After incubation at various temperatures for 60 min, the cells were fixed and stained with DRAQ5 and an antibody recognizing endogenous Ran (a), Imp β (b), CRM1 (c), or Imp α1 (d and e). Then, N/C intensities were plotted (see also Fig. S1, c and d). Bars, 10 µm. **(f)** After 60 min incubation at indicated temperatures, endogenous HSC70, HSP70, and Imp α1 were detected using WB. **(g–l)** Cells transfected with either negative control (g and j), Hikeshi 2 (h and k), or Hikeshi 3 (i and l) siRNA-treated cells were incubated at various temperature for 60 min. Then, the cells were stained with either anti-HSC/HSP70 (g–i) or anti–Imp α1 (j–l) antibodies, and N/C intensities at each temperature were plotted. Black bars show the median of >50 cells at eight temperature conditions (total *n* = 521 [a], 478 [b], 513 [c], 462 [e], 500 [g], 467 [h], 502 [i], 460 [j], 462 [k], and 463 [l]). All plots in each graph were calculated from one simultaneous experiment. Red lines show threshold temperatures.

NLS [SV NLS], hM9 NLS, and HIV-1 Rev protein [Rev] NES). Because these probes are small enough to pass through NPCs diffusively (Paine et al., 1975), when Ran-dependent active transport is completely inhibited, these transport probes ideally distribute throughout the cells. In fact, GFP-SV NLS and GFP-Rev NES, which are Imp α/β–dependent import and CRM1-dependent export cargoes, distributed equally between the nucleus and cytoplasm after incubation on ice, whereas NLS and NES probes accumulated in the nucleus and the cytoplasm, respectively, at 37.3°C (Fig. 2, a and c). Only GFP-hM9 NLS, which is a transportin-dependent import cargo, was partially retained in the nucleus even after incubation on ice, probably because of its energy-independent binding to the nuclear interior (Fig. 2 b). Using these cell lines, we performed temperature-shift assays (Fig. 2).

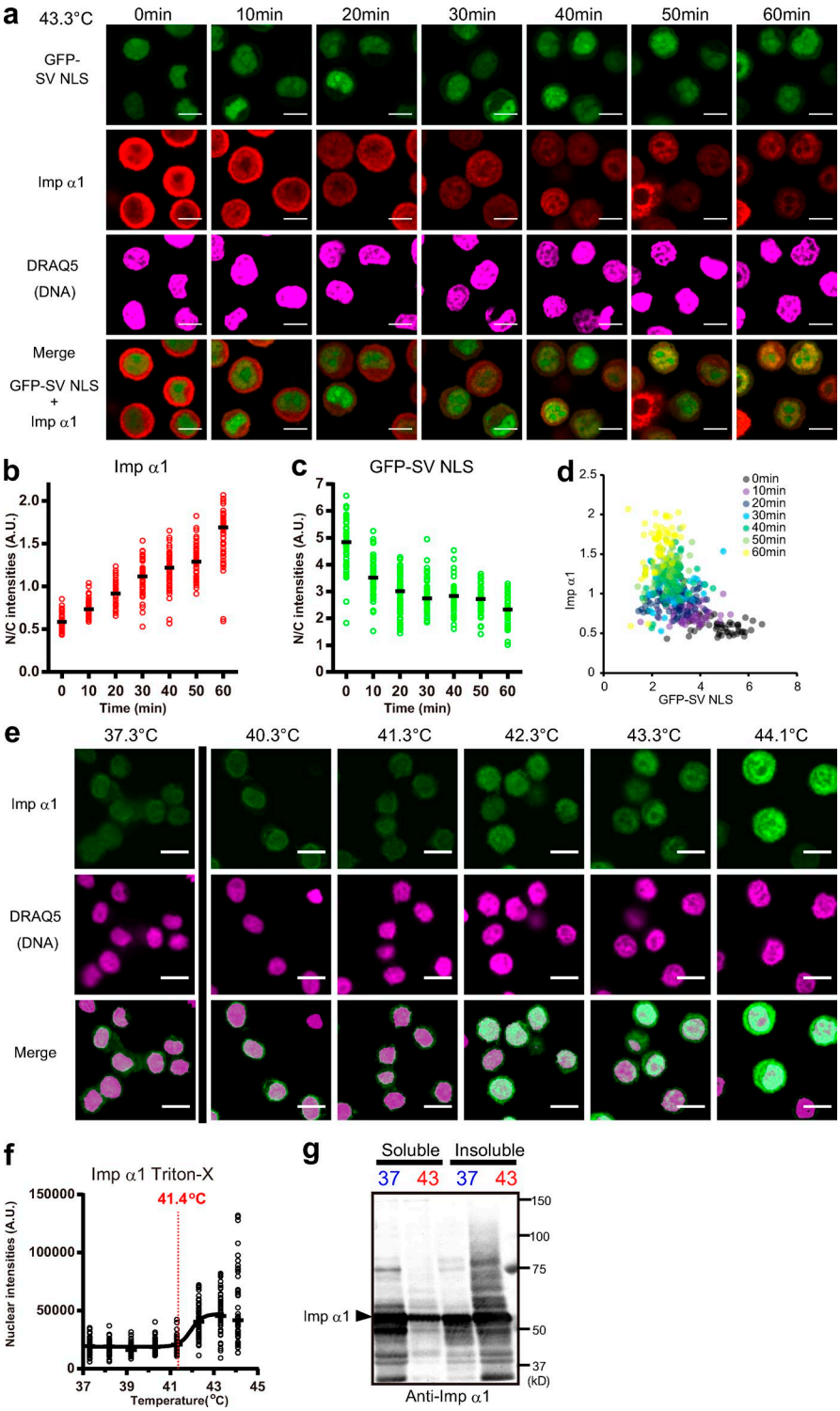

Figure 4. **Relationship between Imp α/β–dependent import and nuclear translocation of Imp α1. (a)** After the incubation at 43.3°C, GFP-SV NLS–expressing stable HeLa S3 cells were fixed at various time points and stained with anti–Imp α1 antibody and DRAQ5 and observed. **(b and c)** The N/C intensities of Imp α1 (b) and GFP-SV NLS (c) versus time (min) were plotted. **(d)** Scatter plots of the nuclear accumulation levels of GFP-SV NLS versus endogenous Imp α1. On the x and y axes, N/C intensities of GFP-SV NLS and Imp α1 are shown, respectively. **(e)** The cells were incubated for 60 min at indicated temperatures, and the cells were permeabilized using ice-cold Triton X-100 and washed out soluble fractions. Then, the cells were fixed and stained with anti–Imp α1 and DRAQ5. Bars, 10 µm. **(f)** Nuclear intensities of insoluble Imp α1 were plotted. Black bars show the median of >50 cells at each temperature. Black bars show the median of >50 cells at seven time points (b and c) or eight temperature conditions (f; total n = 424 [b–d] and 445 [f]). All plots in each graph were calculated from one simultaneous experiment. The red line in f shows the threshold temperature. **(g)** Cells were incubated for 60 min either at 37.3 or 43.3°C and separated into soluble and insoluble fractions. Then, Imp α1 was detected using WB.

The import efficiency of GFP-SV NLS suddenly started to drop at 42.3°C. Similarly, the import efficiency of GFP-fused NLS of CAP-binding protein 80 (CBP80), which is known as a bipartite NLS for Imp α/β–dependent import (Izaurralde et al., 1994; Weis et al., 1995), dropped at 42.3°C (Fig. S1 a). In contrast, the nuclear import of GFP-hM9 NLS was only partially repressed at 43.3°C and was almost inhibited at 44.1°C. The nuclear export of GFP-Rev NES was not affected at ≤43.3°C and was only partially inhibited at 44.1°C.

Fig. 2 g summarizes the different temperature dependencies of nuclear transport systems. The nuclear translocations of HSP70s (threshold temperature 39.9°C and 39.7°C), the inhibition of Imp α/β–dependent import (threshold temperature 41.5°C), and suppression of other Ran-dependent transport (threshold temperature of hM9 NLS and Rev NES were 42.6°C and 43.8°C, respectively) occur in order from low to high temperature. This indicates that the nuclear transport system responds to the temperature rise in a multistep mechanism in accordance

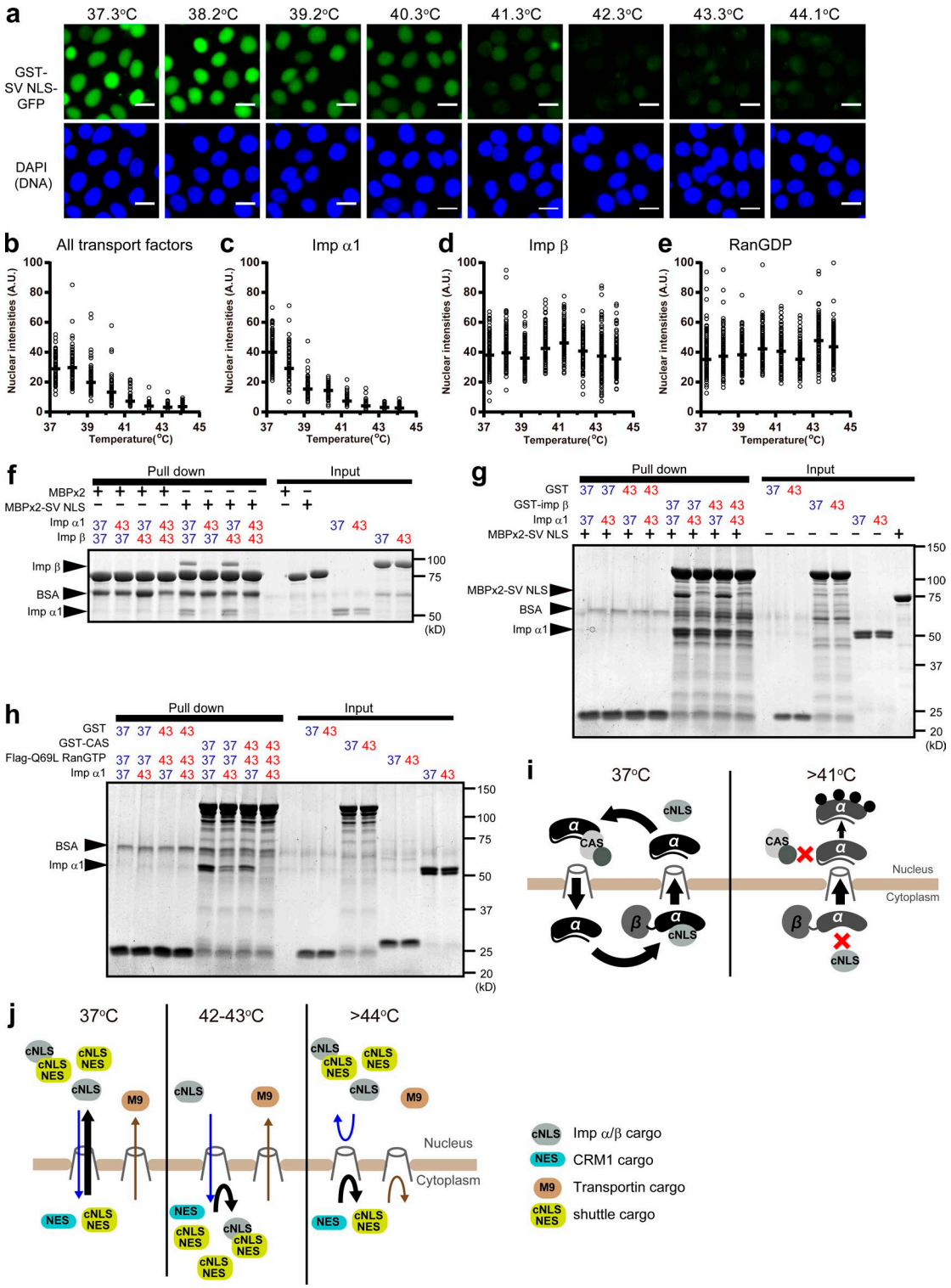

Figure 5. **Thermosensitivity of Imp α1. (a and b)** Using Imp α1, Imp β, and RanGDP preincubated at indicated temperatures, in vitro transport assays of GST-SV NLS–GFP were performed. After the reactions, the cells were fixed and stained with DAPI (a). Then, nuclear intensities of GST-SV NLS–GFP were plotted (b). Bars, 20 µm. **(c–e)** Imp α1 (c), Imp β (d), or RanGDP (e) was preincubated for 60 min at indicated temperatures, and the remaining two transport factors were preincubated at 37.3°C. Then, the import assays of GST-SV NLS–GFP were performed. The nuclear intensities were plotted (see also Fig. S3, a–c). Black bars show the median of >100 cells at eight temperature conditions (total *n* = 1,521 [b], 1,255 [c], 1,598 [d], and 1,494 [e]). All plots in each graph were calculated from one simultaneous experiment. **(f)** Imp α1 and Imp β were independently preincubated at either 37.3 or 43.3°C for 60 min. Then, these proteins and either MBPx2 or MBPx2-SV NLS were incubated with amylose beads. **(g)** GST, GST–Imp β, and Imp α1 were independently preincubated at either 37.3 or 43.3°C. Then, either GST or GST–Imp β was incubated with Imp α1, MBPx2-SV NLS, and glutathione beads. **(h)** GST, GST-CAS, Flag-RanGTP (Q69L), and Imp α1 were independently preincubated at either 37.3 or 43.3°C. Then, either GST or GST-CAS was incubated with Imp

with the degree of stress. These multistep inhibitions of Ran-dependent transport were also observed in the noncancer cell line human telomerase immortalized retinal pigment epithelial cell (hTERT)-RPE1 (Fig. S1 a).

Next, we analyzed localizations of transport factors. It has been previously reported that Ran leaks from the nucleus (Furuta et al., 2004; Miyamoto et al., 2004; Yasuda et al., 2006) under higher temperatures, but quantification of the nuclear versus cytoplasmic (N/C) intensities revealed that such leakage is slight (Fig. 3 a). Thus, we suspect that the Ran gradient between the cytoplasm and nucleoplasm was maintained to some extent at temperatures below ∼44°C. The localization of Imp β and CRM1 was also mostly unaffected by temperature rise (Fig. 3, b and c). These results are consistent with earlier-described results that transportin- and CRM1-dependent transport, which are mediated by only Imp β family proteins and Ran, were only partially inhibited at temperatures <44°C (Fig. 2, e–g).

In contrast, Imp α, which is an adapter molecule for formation of import complexes with Imp β and basic NLS substrates, has been reported to translocate into the nucleus in response to heat, oxidative, and UV stress (Furuta et al., 2004; Miyamoto et al., 2004; Yasuda et al., 2012). As expected, the localization of Imp α1 shifted into the nucleus according to temperature rise (Fig. 3, d and e). Although Imp α1 was mainly localized in the cytoplasm at ≤40.2°C, it showed sudden shift in translocation into the nucleus at ≥42.3°C. The calculated threshold temperature of Imp α1 nuclear translocation was 41.5°C and completely matched the threshold temperature of Imp α/β–dependent import inhibition (Fig. 2 d). Although total intensities of endogenous Imp α1 detected by immunostaining decreased at 43.3 and 44.1°C (Figs. 3 d and S1 e), the total protein amount of Imp α1 did not decrease significantly in Western blot (WB) analysis (Fig. 3 f). Therefore, in immunostaining, the accessibility of the antibody to epitopes on endogenous Imp α1 molecules may be different after being exposed to high temperatures. Additionally, in WB analysis of Imp α1, higher-molecular weight forms were observed at temperatures <41.3°C (Fig. 3 f). These bands may be modified forms of Imp α1 because they disappeared in Imp α1–knockdown cells (Fig. S1 f). The nuclear translocation of Imp α1 was not affected by knockdown of Hikeshi, which is an HSP70s-specific transport factor (Fig. 3, g–l). Thus, the nuclear translocation of Imp α1 is independent of that of HSP70s under high-temperature conditions.

For detailed analysis of relationships between the inhibition of import and the nuclear translocation of Imp α1, we examined immunofluorescence (IF) of endogenous Imp α1 in GFP-SV NLS–expressing cells at various time points (Fig. 4 a; see also Fig. S2). Upon an increase in temperature to 43.3°C, Imp α1 translocated into the nucleus (Fig. 4 b), and the import of GFP-SV NLS was gradually suppressed (Fig. 4 c). The scatter plot of the N/C intensities of Imp α1 versus those of GFP-SV NLS shows the inhibition of GFP-SV NLS import occurs in inverse proportion to the nuclear translocations of Imp α1 (Fig. 4 d). Therefore, nuclear translocation of Imp α1 seems to induce the suppression of Imp α/β–dependent import.

It has been reported that after heat stress, nuclear Imp α is retained at nuclear structures (Furuta et al., 2004; Miyamoto et al., 2004). Therefore, we expected that under high temperatures, nuclear Imp α1 would be sequestered by binding to intranuclear structures. To verify this, we analyzed cells at temperatures that allow nuclear retention of Imp α1. After temperature shift for 60 min, the cells were permeabilized with Triton X-100, and the soluble fractions were washed out. Then, the cells were fixed, and endogenous Imp α1 that remained bound to intracellular structures was stained (Fig. 4 e). As expected, the nuclear retention of Imp α1 increased at higher temperatures. Notably, the threshold temperature of the nuclear retention was 41.4°C (Fig. 4 f), which is almost same as the threshold temperatures of the inhibition of Imp α/β import and the nuclear translocation of Imp α1 (41.5°C). At these temperatures, Imp α1 was also retained in the cytoplasm. Indeed, it has been reported that a part of Imp α1 is recruited into cytoplasmic RNA stress granules under heat stress conditions (Fujimura et al., 2010; Mahboubi et al., 2013).

Although the insoluble proportion of Imp α1 cannot participate in nuclear import, part of Imp α1 remains in soluble fractions (Fig. 4 g). To know whether soluble Imp α1 under high temperatures possesses transport ability or not, we performed an in vitro transport assay of GST-SV NLS–GFP in permeabilized adherent HeLa S3 cells at 37°C using recombinant transport factors preincubated at the temperature ranges of 37.3–44.1°C for 60 min. We observed that upon elevating the incubation temperature from 37.3°C to 41.2°C, the import efficiencies gradually decreased, and at temperatures >42.3°C, the import was completely inhibited (Fig. 5, a and b). To identify which factors became dysfunctional at high temperatures, the transport assays were performed using only one of the three transport factors preincubated at the temperature ranges of 37.3–44.1°C and the residual factors preincubated at 37.3°C for 60 min. When either RanGDP or Imp β were preincubated at high temperatures, the nuclear import efficiencies were not affected (Fig. 5, d and e; and Fig. S3, b and c). These results support the hypothesis that RanGTP/GDP cycles between the nucleus and the cytoplasm and that the transport functions of Imp β are stable at the temperature ranges of 37.3–44.1°C. In contrast, when only Imp α1 was preincubated at high temperatures, the import efficiencies dropped drastically (Figs. 5 c and S3 a) in the same manner as observed in Fig. 5 (a and b). These results indicate that the temperature sensitivity of Imp α1 itself is responsible for selective inhibition of Imp α/β–dependent nuclear import. Importantly, it should be noted that we performed the transport assays at 37°C. Therefore, once exposed to high temperatures, Imp α1 becomes irreversibly dysfunctional or takes time to recover the functions.

α1, Flag-RanGTP (Q69L), and glutathione beads. Proteins bound to beads were analyzed by Coomassie brilliant blue staining. **(i)** Model for the inhibition of Imp α/β–dependent import and the nuclear translocation of Imp α. **(j)** Model for temperature-dependent transport modulations. cNLS indicates classical NLS, which is recognized by Imp α1.

To elucidate the cause of the import inhibition, we performed binding assays using recombinant transport factors preincubated at either 37.3 or 43.3°C. After preincubations, Imp α1 and Imp β were mixed with double maltose-binding protein fusion (MBPx2)-SV NLS. When only Imp α1 was preincubated at 43.3°C, the Imp α1/ Imp β heterodimer did not bind to MBPx2-SV NLS (Fig. 5 f). Imp α1 preincubated at 43.3°C still bound to GST-Imp β, whereas MBPx2-SV NLS did not bind to Imp α1 (Fig. 5 g). Therefore, Imp α1 exposed to higher temperatures could still bind to Imp β but not to NLS cargos. Similarly, the binding between Imp α1 preincubated at 43.3°C and MBPx2-CBP80 NLS was also inhibited (Fig. S3 d). Additionally, the formation of Imp α1 export complex with GST–cellular apoptosis sucesptibility (CAS; Kutay et al., 1997; Künzler and Hurt, 1998; Solsbacher et al., 1998) and Ran (Q69L) GTP, which is a GTPase-deficient mutant (Klebe et al., 1995), was inhibited by preincubation at 43.3°C (Fig. 5 h). This indicates that nuclear Imp α1 exposed to high temperatures cannot be exported even if the RanGTP gradient does not collapse. Importantly, Imp β exposed to high temperatures was able to bind Imp α1 (Fig. 5 g) and retained import activity in in vitro transport assays (Fig. 5 d). Therefore, at high temperatures, Imp α1 seemed to translocate into the nucleus at least in an Imp β–dependent manner, whereas its export was inhibited (Fig. 5 h), resulting in Imp α1 accumulation into the nucleus in high temperatures (Fig. 5 i).

In this study, we showed that responses of individual transport pathways upon elevating temperatures are initiated at different thresholds (Fig. 2 g). Especially, we found that the inhibition of Imp α/β–dependent import at lower temperature is caused by thermosensitivity of Imp α1. In this study, we analyzed only Imp α1, which is one of seven human Imp α subtypes (Goldfarb et al., 2004; Alvisi and Jans, 2015; Pumroy and Cingolani, 2015; Miyamoto et al., 2016). The thermosensitivities may be different among subtypes and may contribute to characterization of the thermotolerance of the cell types.

Shutdown of only one of the import pathways may affect nuclear content of proteins according to temperature rise (Fig. 5 j). There are many nucleocytoplasmic shuttling proteins, which contain both NES and Imp α/β–dependent NLS sequences, in complex with other proteins in the nucleus. These protein complexes may translocate into the cytoplasm at temperature ranges of ∼42–43°C because Imp α/β–dependent import is inhibited, whereas CRM1-dependent export is still active. However, transportin-dependent import is active up to ∼43°C. Therefore, types of localization signal could specify localization change of proteins according to the strength of heat stress. In addition to Imp α/β–, transportin-, and CRM1-dependent transport, several other transport pathways that have different thermal sensitivities may conduct specific functions. Because in some cases cargoes of the same transport factors are linked to distinct biological processes (Kimura et al., 2017), protein groups may use multiple import pathways differentially depending on their necessity for various intranuclear stress responses (Kimura and Imamoto, 2014). Therefore, these regulatory changes in transport may have an important role for progressing intranuclear stress response. Our findings will lead to a better understanding of how cells protect against stress by nuclear functions.

Materials and methods

Cell culture

HeLa S3 cells in suspension culture conditions were grown in RPMI 1640 supplemented with 5% FBS at 37°C with 5% CO_2 in noncoated dishes. HeLa S3 cells in adherent culture conditions and hTERT-RPE1 were grown in DMEM supplemented with 10% FBS at 37°C with 5% CO_2 in tissue culture–treated dishes.

DNA plasmids

For transfection, the BglII–EcoRI fragment of CBP80 NLS (CYM SRRRHSDENDGGQPHKRRKTSDANETED; Miyamoto et al., 1997) and the BamHI–EcoRI fragments of SV NLS (PKKKRKV; Kalderon et al., 1984), hPY-NLS of hnRNP A1 (hM9NLS; GGSYNDFGN YNNQSSNFGPMKGGNFGGRSSGPYGGGGQY; Cansizoglu et al., 2007) and HIV-1 Rev NES (DVSDLPPLERLTLRGG; Güttler et al., 2010) were inserted into the BglII and EcoRI sites of mammalian expression vector pEGFP-C1 (6086-1; Takara Bio Inc.).

For recombinant protein purification, the following constructs were used: GST-SV NLS–GFP, Flag-Ran (Q69L), and Ran (human) were generated by inserting BamHI–EcoRI fragments into BamHI–EcoRI sites of the *Escherichia coli* N-terminal GST-fused protein expression vector pGEX-2T (GE Healthcare). Imp α1 (human), Imp β (human), and CAS (human) were generated by inserting BamHI–XhoI fragments into the BamHI and XhoI sites of the *E. coli* GST-fused protein expression vector pGEX-6P-1 (GE Healthcare). The pMALx2-C vector for expression of MBPx2 was generated by inserting EcoRI–HindIII PCR fragment of MBP into EcoRI and HindIII sites of *E. coli* MBP-fused protein expression vector pMAL-C (New England Biolabs, Inc.). Then, BamHI–EcoRI fragments of the SV NLS BglII–EcoRI fragment of CBP80 NLS were inserted into BamHI and EcoRI sites of pMALx2-C.

Plasmid transfection and generating stable cell lines

All plasmids were transfected into cells using Effectene transfection reagent (301425; QIAGEN). For establishment of HeLa S3 stable cell lines, after 48 h, transfected cells were grown in DMEM supplemented with 10% FBS, 800 µg/ml G418, and 0.65% methylcellulose (138-05052; Wako Pure Chemical Industries) for 2–3 wk. Then, fluorescent positive colonies were picked up. For establishment of hTERT-RPE1 stable cell lines, the cells were transfected in a six-well dish. After 72 h, cells were seeded into two 100-mm dishes. After 24 h, G418 was added to the medium at a final concentration of 1,000 µg/ml and grown for 11–13 d. Then, fluorescent positive colonies were picked up.

Recombinant protein expression and purification

Transformation of *E. coli* expression vectors, protein expression, bacterial cell lysis, and protein purification were performed as described previously (Imamoto et al., 1995; Miyamoto et al., 2002). Essentially, plasmids for recombinant proteins were transformed in the *E. coli* BL21 strain. After culture at 37°C for 4–6 h, recombinant proteins were expressed by addition of 0.1 mM IPTG at 18°C overnight. The bacteria pellets were suspended in lysis buffer (50 mM Tris-HCl, pH 8.3, 500 mM NaCl, and 1 mM EDTA, pH 8.0) and lysed by freezing, thawing, and sonication. After centrifuging at 20,000 rpm, the supernatants were mixed with glutathione Sepharose (17-0756-05; GE Healthcare) for GST-fused proteins or

amylose beads (E8021; New England Biolabs, Inc.) for MBP-fused proteins. GST, GST–Imp β, GST-CAS, and GST-SV NLS–GFP were eluted by addition of 10 mM reduced glutathione in PBS⁻. Imp α1 and Imp β were purified by cleaving off the N-terminal GST tag using PreScission protease (27084301; GE Healthcare) at 80 U/ml beads. Flag-Ran (Q69L) and Ran were purified by cleaving off the N-terminal GST tag using thrombin (T7513; Sigma-Aldrich) at 80 U/ml beads. MBPx2, MBPx2-SV NLS, and MBPx2-CBP80 NLS were eluted by addition of 100 mM maltose monohydrate (136-00612; Wako Pure Chemical Industries) in column buffer (20 mM Tris-HCl, 200 mM NaCl, and 1 mM EDTA). GTP-bound Flag-Ran (Q69L) and GDP-bound Ran were purified as described previously (Sekimoto et al., 1996). Essentially, 25 mM EDTA and 2 mM GTP (for Flag-Q69LRan GTP) or GDP (for Ran GDP) were added to Ran (Q69L) or Ran (WT), and after incubation for 1 h on ice, $MgCl_2$ was added at a final concentration of 50 mM.

RNAi

Transfection of siRNA was performed using RNAi MAX (13778150; Thermo Fisher Scientific) according to the manufacturer's protocol for reverse transfection. The following siRNA duplexes were purchased from QIAGEN: siRNA Imp α1 2 (5′-CAG UGGUGGAACAGUUGAATT-3′), siRNA Imp α1 3 (5′-GUGUUCCGA GACUUGGUUATT-3′), siRNA Hikeshi 2 (5′-CAGCAAGUGGCAGAG GAUAAA-3′), and siRNA Hikeshi#3 (5′-CUCCUAGGAUUUGUC ACGAAU-3′). Universal negative control siRNA was purchased from NIPPON GENE.

Temperature stability test

Temperature stability test of each well in the thermal cycler was performed using thermologger (AM-8000; ANRITSU) with a high-accuracy thermosensor (S16299; ANRITSU). The thermosensor was inserted into a PCR tube with 50 µl of water and set in the thermal cycler. The well temperature was plotted every second over 1 h.

IF of suspension culture cells after temperature-shift assay

Suspension cultures of HeLa S3 cells were prepared at a concentration of 3 × 10^6 cells per ml in RPMI 1640 medium supplemented with 5% FBS and 20 mM Hepes, pH 7.3. After preparation of thermal programs of the thermal cycler (TP350; Takara Bio Inc.), 50 µl of the cell suspensions was applied in each PCR tube. Top heater temperatures of all thermal programs were set at 60°C. At each time point, 16 µl of 16% formaldehyde in PBS⁻ was added (final concentration 3.9%). After incubation for 10 min, 5.4 µl of 2 M glycine was added (final concentration 151 mM) to quench the excess of formaldehyde. After washing with PBS⁻ five times, the cells were resuspended in ∼20 µl of PBS⁻. Then, the cells were applied on MAS-coated multiwell plates (TF2404M; MATSUNAMI GLASS) and incubated for at least 10 min at room temperature. After unbound cells were washed out with PBS⁻, IF experiments were performed.

The cells were permeabilized with 0.5% Triton X-100 in PBS⁻ for 10 min followed by 1–2 h incubation in 5% skim milk in PBS⁻ at room temperature. Incubations with primary antibodies were performed in 5% skim milk in PBS⁻ either at room temperature for 2–3 h or at 4°C overnight. After a wash with PBS⁻ three times, incubations with secondary Alexa Fluor–conjugated antibodies were performed at room temperature for 1–2 h. After wash with PBS⁻, the samples were incubated in transport buffer (20 mM Hepes-NaOH, pH 7.3, 110 mM potassium acetate, 2 mM magnesium acetate, 5 mM sodium acetate, and 2 mM EGTA-NaOH, pH 7.3) for 30 min at room temperature followed by incubation in 2.5 µM DRAQ5 (DR50050; Biostatus) in transport buffer for 30 min at 37°C. After washing with transport buffer twice, the samples were mounted with ProLong diamond antifade mounting medium (P36961; Thermo Fisher Scientific). Incubation of cells using a conventional water bath was performed as follows. The cells were grown on 24-well glass-bottomed plates. The next day, the plates were incubated in a water bath preset at various temperatures for 60 min. After incubation, the cells were fixed with 3% formaldehyde in PBS⁻ at 37°C for 10 min.

Preparation of permeabilized cells using Triton X-100

After temperature shift assays, 20 µl of cell suspension was spotted on a MAS-coated multiwell plate and incubated for 5 min at room temperature. Then, the plate was permeabilized with ice-cold 0.1% Triton X-100 in PBS⁻ for 10 min on ice. After washing with ice-cold PBS⁻, the cells were incubated with ice-cold 2% BSA in PBS⁻ for 10 min. After washing with PBS⁻ again, the cells were fixed with 3.7% formaldehyde in PBS⁻ at room temperature for 10 min.

Preparation of whole-cell lysates

After a temperature-shift assay using the thermal cycler, the cells were washed once with PBS⁻ and then immediately lysed in cell lysis buffer (50 mM Tris-HCl, pH 8.0, 0.5% SDS, and 1 mM DTT). Then, the lysates were incubated at 95°C for 10 min and centrifuged at 15,000 rpm for 10 min. Finally, 6× sample buffer was added to the lysates.

Antibodies

The antibodies used in this study were as follows: mouse anti–Imp α1 (610486; BD) at 1:500 for both WB and IF, mouse anti-HSC/HSP70 (1H5; NBP2-02244; Novus Biologicals) at 1:1,000 for both WB and IF, mouse anti-HSP70 (C92F3A-5; BML-SA660; Enzo Life Sciences) at 1:1,000 for both WB and IF, mouse anti–β-actin (AC-15; A-5441; Sigma-Aldrich) at 1:5,000 for WB, mouse anti-Ran (610341; BD) at 1:500 for IF, and rabbit anti-CRM1 (sc-5595; Santa Cruz Biotechnology, Inc.) at 1:100 for IF.

The secondary antibodies used for IF were as follows: donkey anti–rabbit IgG–Alexa Fluor 488 (ab150061; Abcam), goat anti–mouse IgG–Alexa Fluor 488 (A-11029; Thermo Fisher Scientific), and goat anti–mouse IgG–Alexa Fluor 594 (A-11032; Thermo Fisher Scientific) at 1:200.

Fractionation

At the concentration of 3 × 10^6 cells per ml, 4.8 × 10^6 cells were incubated at either 37.3 or 43.3°C for 60 min using the thermal cycler. Then, the cells were immediately placed on ice and washed twice with ice-cold PBS⁻. Then, the cells were suspended in 500 µl lysis buffer (0.5% Triton X-100, 20 mM *N*-ethylmaleimide, and protease inhibitor cocktail [11873580001; Roche] in PBS⁻) and rotated for 20 min at 4°C. After centrifugation, the supernatants

were collected as soluble fractions. Remaining insoluble materials were resuspended in 500 µl of fresh lysis buffer and briefly sonicated. After centrifugation at 21,500 *g* for 10 min at 4°C, the supernatants were collected as the insoluble fractions.

In vitro transport assay

Imp α1, Imp β, and RanGDP recombinant proteins were independently preincubated for 60 min at indicated temperatures using the thermal cycler at the concentrations of 6 µM, 4 µM, and 40 µM in transport buffer, respectively. Preparation of semiintact HeLa S3 cells was performed as described previously (Ogawa et al., 2012). Essentially, HeLa S3 cells in adherent culture conditions were grown on multiwell plates (TF2404; MATSUN AMI GLASS) for 2 d. After washing with ice-cold transport buffer, HeLa S3 cells were incubated in ice-cold transport buffer containing 20 µg/ml digitonin for 5 min. Cells were then washed and incubated in fresh ice-cold transport buffer for 10 min. The resulting semiintact cells were used for in vitro transport assays. Preincubated 600 nM Imp α1, 400 nM Imp β, and 4 µM RanGDP were mixed with 800 nM GST-SV NLS–GFP, 500 µM GTP, and an ATP regeneration system (3.3 µM ATP, 15 µM phosphocreatine, and 60 U/ml creatine phosphokinase) in transport buffer containing 1% BSA. The mixtures were added to semiintact cells and incubated at 37°C for 20 min. Cells were then washed with transport buffer and fixed with 3.7% formaldehyde in transport buffer. Then, the cells were stained with DAPI.

Binding assay

Imp α1, Imp β, GST, GST-Imp β, GST-CAS, and Flag-Ran (Q69L) GTP were preincubated at indicated temperatures for 60 min at the concentrations of 10 µM in transport buffer using the thermal cycler. Then, the recombinant proteins were added into ice-cold transport buffer containing 1% BSA and either glutathione Sepharose beads (17075605; GE Healthcare) for GST-fused proteins or amylose beads (E8021; New England Biolabs, Inc.) for MBP-fused proteins. The mixtures were rotated at 4°C for 60 min and then washed with ice-cold transport buffer three times.

Fluorescence microscopy and data analysis

Confocal imaging was performed at room temperature with an FV1200 microscope equipped with Multi-Alkali photomultiplier tube detector (Olympus). Imaging of GFP, Alexa Fluor 594, and DRAQ5 in Figs. 1, 2, 3, and 4 were obtained using oil-immersion objective lenses (UPlan S-Apochromat 100× oil, 100× 1.40 NA [Olympus]; immersion oil n = 1.516 [GE Healthcare]; 200-µm pinhole). Imaging in Fig. S1 a was obtained using oil-immersion objective lenses (Plan Apochromat 60× oil, 60× 1.42 NA [Olympus]; immersion oil n = 1.516; 100-µm pinhole). All confocal imaging acquisitions were performed using FV10-ASW (4.02; Olympus). Imaging of transport assay in Figs. 5 and S3 was carried at room temperature with a BX51 upright microscope (Olympus) equipped with UPlan Apochromat 20× 0.70 NA objective lens (20× 0.17 NA; Olympus) and a mercury lamp. Fluorescence images of GFP and DAPI were detected with an ORCA-ER charge-coupled device camera (C4742-95; Hamamatsu Photonics). All imaging acquisitions were performed using MetaVue (6.2r6; Molecular Devices).

All analyses of fluorescence-based localizations were performed using the image analysis software ImageJ (National Institutes of Health). Series of single-channel images were not processed any imaging operations but set at the same contrast. Merged images with DRAQ5 or DAPI staining were obtained from magenta binary image of DRAQ5 or DAPI staining and GFP or Alexa Fluor 488 staining images adjusted to proper contrast ranges. All statistical analyses and graph drawing were performed using Excel (2013; Microsoft) and Prism 5 (GraphPad Software).

To calculate N/C mean intensities of individual cells, cytoplasmic and nuclear regions were determined using ImageJ. Nuclear regions were determined from DRAQ5- or DAPI-stained images by threshold default setting automatically. Cytoplasmic regions were determined from differential interference contrast images manually. Then, mean fluorescence intensities and areas of the entire cell and its nucleus were measured from fluorescent images as I_{Total}, I_{Nuc}, S_{Nuc}, and S_{Total}, respectively. Background mean intensity of each image was measured at outside of cells as I_{Back}. Using Excel, N/C intensity N was calculated as below:

$$N = (I_{Nuc} - I_{Back})^{*}(S_{Total} - S_{Nuc}) \,/\, ([I_{Total} - I_{Back})]^{*}S_{Total} - [I_{Nuc} - I_{Back}]^{*}S_{Nuc}).$$

The calculated values were then made into scatter plots using Excel or Prism. To determine the threshold temperature, the plots were fitted to the following sigmoid function using Prism.

$$N(T) = N_{bottom} + (N_{top} - N_{bottom})/(1 + 10^{[T_{50\%}-T]^{*}H})$$

N_{top} and N_{bottom} are mean maximum and minimum N/C intensities. $T_{50\%}$ means the temperature just in the middle of the maximum and minimum N/C intensities. H means the hill slope at $T_{50\%}$. The temperature at which the ratio changed by 10% defined as the threshold temperature. All plots except those in Fig. 2 (d–f) were fitted without any constraint. For better fitting, N_{bottom} of GFP-SV NLS (Fig. 2 d) and GFP-hM9 NLS (Fig. 2 e) and N_{top} of GFP-RevNES (Fig. 2 f) were used median values on ice.

Online supplemental material

Fig. S1 (a and b) explains temperature dependencies of transport in hTERT-RPE1 cells stably expressing GFP-fused NLS and NES using a conventional water bath. Fig. S1 (c and d) shows that the localizations of endogenous Ran in HeLa S3 suspension culture conditions are partially different from those in adhesive cultured cells. Fig. S1 e shows that immunofluorescent intensities of Imp α1 decrease under high temperatures. Fig. S1 f shows that high–molecular weight bands of Imp α1 disappear in Imp α1 knockdown cells, meaning these bands seem to be not nonspecific or cross-reacted proteins. Fig. S2 shows that relationships between nuclear accumulations of Imp α1 and the inhibitions of GFP-SV NLS at 42.3 and 44.1°C are similar to Fig. 4 (b–d). Fig. S3 (a–c) shows representative images in Fig. 5 (c–e). Fig. S3 d shows thermosensitivity of bindings between Imp α1 and CBP80 NLS.

Acknowledgments

We thank members of the Cellular Dynamics laboratory for their helpful discussions.

This work was supported by Japan Society for the Promotion of Science KAKENHI grants JP15H05929 and JP25871121 and the RIKEN Pioneering research project (Cellular Evolution).

The authors declare no competing financial interests.

Author contributions: Y. Ogawa designed and performed experiments, analyzed all the data, wrote the manuscript. N. Imamoto helped with the experimental design, wrote the manuscript, and directed the project.

Submitted: 8 December 2017
Revised: 6 April 2018
Accepted: 20 April 2018

References

Alvisi, G., and D.A. Jans. 2015. Basis of cargo recognition by importin αs: the power of structure. *Structure.* 23:251–252. https://doi.org/10.1016/j.str.2015.01.005

Cansizoglu, A.E., B.J. Lee, Z.C. Zhang, B.M. Fontoura, and Y.M. Chook. 2007. Structure-based design of a pathway-specific nuclear import inhibitor. *Nat. Struct. Mol. Biol.* 14:452–454. https://doi.org/10.1038/nsmb1229

Chook, Y.M., and K.E. Süel. 2011. Nuclear import by karyopherin-βs: recognition and inhibition. *Biochim. Biophys. Acta.* 1813:1593–1606. https://doi.org/10.1016/j.bbamcr.2010.10.014

Cronshaw, J.M., A.N. Krutchinsky, W. Zhang, B.T. Chait, and M.J. Matunis. 2002. Proteomic analysis of the mammalian nuclear pore complex. *J. Cell Biol.* 158:915–927. https://doi.org/10.1083/jcb.200206106

Datta, S., C.J. Snow, and B.M. Paschal. 2014. A pathway linking oxidative stress and the Ran GTPase system in progeria. *Mol. Biol. Cell.* 25:1202–1215. https://doi.org/10.1091/mbc.E13-07-0430

Daugaard, M., M. Rohde, and M. Jäättelä. 2007. The heat shock protein 70 family: Highly homologous proteins with overlapping and distinct functions. *FEBS Lett.* 581:3702–3710. https://doi.org/10.1016/j.febslet.2007.05.039

Fujimura, K., T. Suzuki, Y. Yasuda, M. Murata, J. Katahira, and Y. Yoneda. 2010. Identification of importin alpha1 as a novel constituent of RNA stress granules. *Biochim. Biophys. Acta.* 1803:865–871. https://doi.org/10.1016/j.bbamcr.2010.03.020

Furuta, M., S. Kose, M. Koike, T. Shimi, Y. Hiraoka, Y. Yoneda, T. Haraguchi, and N. Imamoto. 2004. Heat-shock induced nuclear retention and recycling inhibition of importin alpha. *Genes Cells.* 9:429–441. https://doi.org/10.1111/j.1356-9597.2004.00734.x

Goldfarb, D.S., A.H. Corbett, D.A. Mason, M.T. Harreman, and S.A. Adam. 2004. Importin alpha: a multipurpose nuclear-transport receptor. *Trends Cell Biol.* 14:505–514. https://doi.org/10.1016/j.tcb.2004.07.01615350979

Görlich, D., and U. Kutay. 1999. Transport between the cell nucleus and the cytoplasm. *Annu. Rev. Cell Dev. Biol.* 15:607–660. https://doi.org/10.1146/annurev.cellbio.15.1.607

Güttler, T., T. Madl, P. Neumann, D. Deichsel, L. Corsini, T. Monecke, R. Ficner, M. Sattler, and D. Görlich. 2010. NES consensus redefined by structures of PKI-type and Rev-type nuclear export signals bound to CRM1. *Nat. Struct. Mol. Biol.* 17:1367–1376. https://doi.org/10.1038/nsmb.1931

Hartl, F.U., A. Bracher, and M. Hayer-Hartl. 2011. Molecular chaperones in protein folding and proteostasis. *Nature.* 475:324–332. https://doi.org/10.1038/nature10317

Imamoto, N., T. Shimamoto, T. Takao, T. Tachibana, S. Kose, M. Matsubae, T. Sekimoto, Y. Shimonishi, and Y. Yoneda. 1995. In vivo evidence for involvement of a 58 kDa component of nuclear pore-targeting complex in nuclear protein import. *EMBO J.* 14:3617–3626.

Izaurralde, E., J. Lewis, C. McGuigan, M. Jankowska, E. Darzynkiewicz, and I.W. Mattaj. 1994. A nuclear cap binding protein complex involved in pre-mRNA splicing. *Cell.* 78:657–668. https://doi.org/10.1016/0092-8674(94)90530-4

Kalab, P., K. Weis, and R. Heald. 2002. Visualization of a Ran-GTP gradient in interphase and mitotic Xenopus egg extracts. *Science.* 295:2452–2456. https://doi.org/10.1126/science.1068798

Kaláb, P., A. Pralle, E.Y. Isacoff, R. Heald, and K. Weis. 2006. Analysis of a RanGTP-regulated gradient in mitotic somatic cells. *Nature.* 440:697–701. https://doi.org/10.1038/nature04589

Kalderon, D., B.L. Roberts, W.D. Richardson, and A.E. Smith. 1984. A short amino acid sequence able to specify nuclear location. *Cell.* 39:499–509. https://doi.org/10.1016/0092-8674(84)90457-4

Kelley, J.B., and B.M. Paschal. 2007. Hyperosmotic stress signaling to the nucleus disrupts the Ran gradient and the production of RanGTP. *Mol. Biol. Cell.* 18:4365–4376. https://doi.org/10.1091/mbc.E07-01-0089

Kimura, M., and N. Imamoto. 2014. Biological significance of the importin-β family-dependent nucleocytoplasmic transport pathways. *Traffic.* 15:727–748. https://doi.org/10.1111/tra.12174

Kimura, M., Y. Morinaka, K. Imai, S. Kose, P. Horton, and N. Imamoto. 2017. Extensive cargo identification reveals distinct biological roles of the 12 importin pathways. *eLife.* 6:e21184. https://doi.org/10.7554/eLife.21184

Klebe, C., F.R. Bischoff, H. Ponstingl, and A. Wittinghofer. 1995. Interaction of the nuclear GTP-binding protein Ran with its regulatory proteins RCC1 and RanGAP1. *Biochemistry.* 34:639–647. https://doi.org/10.1021/bi00002a031

Kodiha, M., P. Bański, D. Ho-Wo-Cheong, and U. Stochaj. 2008. Dissection of the molecular mechanisms that control the nuclear accumulation of transport factors importin-alpha and CAS in stressed cells. *Cell. Mol. Life Sci.* 65:1756–1767. https://doi.org/10.1007/s00018-008-7588-2

Kose, S., M. Furuta, and N. Imamoto. 2012. Hikeshi, a nuclear import carrier for Hsp70s, protects cells from heat shock-induced nuclear damage. *Cell.* 149:578–589. https://doi.org/10.1016/j.cell.2012.02.058

Künzler, M., and E.C. Hurt. 1998. Cse1p functions as the nuclear export receptor for importin alpha in yeast. *FEBS Lett.* 433:185–190. https://doi.org/10.1016/S0014-5793(98)00892-8

Kutay, U., F.R. Bischoff, S. Kostka, R. Kraft, and D. Görlich. 1997. Export of importin alpha from the nucleus is mediated by a specific nuclear transport factor. *Cell.* 90:1061–1071. https://doi.org/10.1016/S0092-8674(00)80372-4

Mahboubi, H., E. Seganathy, D. Kong, and U. Stochaj. 2013. Identification of Novel Stress Granule Components That Are Involved in Nuclear Transport. *PLoS One.* 8:e68356. https://doi.org/10.1371/journal.pone.0068356

Miyamoto, Y., N. Imamoto, T. Sekimoto, T. Tachibana, T. Seki, S. Tada, T. Enomoto, and Y. Yoneda. 1997. Differential modes of nuclear localization signal (NLS) recognition by three distinct classes of NLS receptors. *J. Biol. Chem.* 272:26375–26381. https://doi.org/10.1074/jbc.272.42.26375

Miyamoto, Y., M. Hieda, M.T. Harreman, M. Fukumoto, T. Saiwaki, A.E. Hodel, A.H. Corbett, and Y. Yoneda. 2002. Importin alpha can migrate into the nucleus in an importin beta- and Ran-independent manner. *EMBO J.* 21:5833–5842. https://doi.org/10.1093/emboj/cdf569

Miyamoto, Y., T. Saiwaki, J. Yamashita, Y. Yasuda, I. Kotera, S. Shibata, M. Shigeta, Y. Hiraoka, T. Haraguchi, and Y. Yoneda. 2004. Cellular stresses induce the nuclear accumulation of importin alpha and cause a conventional nuclear import block. *J. Cell Biol.* 165:617–623. https://doi.org/10.1083/jcb.200312008

Miyamoto, Y., K. Yamada, and Y. Yoneda. 2016. Importin α: a key molecule in nuclear transport and non-transport functions. *J. Biochem.* 160:69–75. https://doi.org/10.1093/jb/mvw036

Ogawa, Y., Y. Miyamoto, M. Oka, and Y. Yoneda. 2012. The interaction between importin-α and Nup153 promotes importin-α/β-mediated nuclear import. *Traffic.* 13:934–946. https://doi.org/10.1111/j.1600-0854.2012.01367.x

Paine, P.L., L.C. Moore, and S.B. Horowitz. 1975. Nuclear envelope permeability. *Nature.* 254:109–114. https://doi.org/10.1038/254109a0

Park, H.G., S.I. Han, S.Y. Oh, and H.S. Kang. 2005. Cellular responses to mild heat stress. *Cell. Mol. Life Sci.* 62:10–23. https://doi.org/10.1007/s00018-004-4208-7

Pumroy, R.A., and G. Cingolani. 2015. Diversification of importin-α isoforms in cellular trafficking and disease states. *Biochem. J.* 466:13–28. https://doi.org/10.1042/BJ20141186

Richter, K., M. Haslbeck, and J. Buchner. 2010. The heat shock response: life on the verge of death. *Mol. Cell.* 40:253–266. https://doi.org/10.1016/j.molcel.2010.10.006

Sekimoto, T., K. Nakajima, T. Tachibana, T. Hirano, and Y. Yoneda. 1996. Interferon-gamma-dependent nuclear import of Stat1 is mediated by the GTPase activity of Ran/TC4. *J. Biol. Chem.* 271:31017–31020. https://doi.org/10.1074/jbc.271.49.31017

Solsbacher, J., P. Maurer, F.R. Bischoff, and G. Schlenstedt. 1998. Cse1p is involved in export of yeast importin alpha from the nucleus. *Mol. Cell. Biol.* 18:6805–6815. https://doi.org/10.1128/MCB.18.11.6805

Stewart, M. 2007. Molecular mechanism of the nuclear protein import cycle. *Nat. Rev. Mol. Cell Biol.* 8:195–208. https://doi.org/10.1038/nrm2114

Weis, K. 2003. Regulating access to the genome: nucleocytoplasmic transport throughout the cell cycle. *Cell.* 112:441–451. https://doi.org/10.1016/S0092-8674(03)00082-5

Weis, K., I.W. Mattaj, and A.I. Lamond. 1995. Identification of hSRP1 alpha as a functional receptor for nuclear localization sequences. *Science.* 268:1049–1053. https://doi.org/10.1126/science.7754385

Welch, W.J., and J.R. Feramisco. 1984. Nuclear and nucleolar localization of the 72,000-dalton heat shock protein in heat-shocked mammalian cells. *J. Biol. Chem.* 259:4501–4513.6368558

Yasuda, Y., Y. Miyamoto, T. Saiwaki, and Y. Yoneda. 2006. Mechanism of the stress-induced collapse of the Ran distribution. *Exp. Cell Res.* 312:512–520. https://doi.org/10.1016/j.yexcr.2005.11.017

Yasuda, Y., Y. Miyamoto, T. Yamashiro, M. Asally, A. Masui, C. Wong, K.L. Loveland, and Y. Yoneda. 2012. Nuclear retention of importin α coordinates cell fate through changes in gene expression. *EMBO J.* 31:83–94. https://doi.org/10.1038/emboj.2011.360

Yoshimura, S.H., S. Otsuka, M. Kumeta, M. Taga, and K. Takeyasu. 2013. Intermolecular disulfide bonds between nucleoporins regulate karyopherin-dependent nuclear transport. *J. Cell Sci.* 126:3141–3150. https://doi.org/10.1242/jcs.124172